Nondiagonal Response of Electrons by Coherent Inelastic X-Ray Scattering *

A. Kaprolat and W. Schülke

Universität Dortmund, Institut für Physik, Postfach 50 05 00, D-W-4600 Dortmund 50

Z. Naturforsch. **48a**, 227–232 (1993); received January 3, 1992

The experimental knowledge of the dielectric response of electrons within a solid is up to now mainly gained by inelastic scattering experiments, using a plane wave as initial state of the probe particle. These experiments allow the measurement of the dynamical structure factor, related to diagonal elements of the inverse dielectric matrix ε^{-1}. We present a new type of scattering experiment that uses as initial state of the probe a standing wave field, thus allowing the experimental determination of *non*-diagonal elements of ε^{-1}. Comparison of the experimental results with a plasmon-band model leads to direct experimental evidence for plasmon-banding in Si.

Key words: Inelastic scattering of X-rays; Dielectric response; Dielectric matrix; Local field effect; Plasmon-band model.

1. Introduction

Conventional **I**nelastic **X**-Ray **S**cattering **S**pectroscopy (**IXSS**) yields information about the macroscopic response function $\mathrm{Im}\,[\varepsilon^{-1}(\boldsymbol{q},\omega)]$ of an electron system. (For a review see, for example, [1].) This quantity, together with the macroscopic dielectric function $\varepsilon(\boldsymbol{q},\omega)$, which can be obtained from $\mathrm{Im}\,[\varepsilon^{-1}(\boldsymbol{q},\omega)]$ by Kramers–Kronig transformation, is important for the quantum-mechanical understanding of a many-body system of interacting particles, as it is related to the exact ground-state energy of such a system including correlation [2], and to the excitation properties. Collective excitations (plasmons) are indicated by poles of $\varepsilon^{-1}(\boldsymbol{q},\omega)$, whereas the electronic band structure, determining the single-particle excitations, can be calculated using a Coulomb interaction, screened by $\varepsilon(\boldsymbol{q},\omega)$ [3]. The **D**ouble-**D**ifferential **S**cattering **C**ross-**S**ection (**DDSCS**) of an IXSS experiment turns out to be connected to the imaginary part of the reciprocal of $\varepsilon(\boldsymbol{q},\omega)$ via the fluctuation-dissipation theorem ([1], (39)).

Considering a real crystalline solid instead of a homogeneous electron gas, we have to introduce the dielectric matrix $\varepsilon_{\boldsymbol{g},\boldsymbol{g}'}(\boldsymbol{q},\omega)$, ($\boldsymbol{g},\boldsymbol{g}'$ being reciprocal-lattice vectors). Thus, the macroscopic dielectric function $\varepsilon^{-1}(\boldsymbol{q},\omega)$ is determined by a diagonal element of the inverse dielectric matrix. This leads to a contribution of all elements of the dielectric matrix (the so-called local field effect) to the experimental information obtained by an IXSS experiment. Collective excitations are no longer coupled to poles of $\varepsilon^{-1}(\boldsymbol{q},\omega)$, but can be calculated from $\det[\varepsilon_{\boldsymbol{g},\boldsymbol{g}'}(\boldsymbol{q},\omega)] = 0$. When in a periodic system there is no longer full translational symmetry, the momentum $\hbar\boldsymbol{q}$ is no longer a conserved quantity, but is defined modulo any reciprocal-lattice vector. A consequence of this fact is the occurrence of plasmon bands [4] in complete analogy to the electron band structure by backfolding of the dispersion relation of plasmons into the 1st Brillouin zone. It seems extremely worthwhile to extend the available experimental information about the dielectric matrix from one diagonal element of the inverse dielectric matrix, as obtained by conventional IXSS experiments, to information about *all* elements of this matrix. In Sect. 2, a new type of inelastic scattering experiment is introduced that, at least in principle, allows us to get this desired information. Section 3 shows an experimental setup and the measuring procedure. In Sect. 4, the experimental results are compared to a theoretical model, the so-called plasmon band model.

* Presented at the Sagamore X Conference on Charge, Spin and Momentum Densities, Konstanz, Fed. Rep. of Germany, September 1–7, 1991.

Reprint requests to Dr. A. Kaprolat, c/o DESY-F41 Hasylab, Notkestr. 85, D-W-2000 Hamburg 52, Fed. Rep. of Germany.

2. Coherent Inelastic X-Ray Scattering

As is shown in more detail in [1], the DDSCS of an IXSS experiment yields the dynamical structure factor

0932-0784 / 93 / 0100-0227 $ 01.30/0. – Please order a reprint rather than making your own copy.

$S(\boldsymbol{q}, \omega)$ via

$$\frac{\mathrm{d}^2\sigma}{\mathrm{d}\omega\,\mathrm{d}\Omega} = \left(\frac{\mathrm{d}\sigma}{\mathrm{d}\Omega}\right)_0 \cdot S(\boldsymbol{q}, \omega)\,, \tag{1}$$

which in turn is related to a diagonal element of the inverse dielectric matrix via

$$S(\boldsymbol{q}, \omega) = -\frac{q^2}{4\pi e^2 n} \cdot \mathrm{Im}\left[\varepsilon^{-1}_{\boldsymbol{g},\boldsymbol{g}'}(\boldsymbol{q}_r, \omega)\right], \tag{2}$$

$$\boldsymbol{q} = \boldsymbol{q}_r + \boldsymbol{g} \in 1^{\mathrm{st}}\ \text{Brillouin zone.}$$

From the definition of ε ([1], (34), (63)) it is known that this quantity connects the Fourier component of an external disturbing potential to the Fourier component of the potential induced within the solid by its response to the external disturbance. Diagonal elements connect Fourier components to the same spatial periodicity, whereas nondiagonal elements connect contributions generated by the microscopic local-field effects in response to the external disturbance. Keeping in mind that transferring *one* momentum $\boldsymbol{q}$ within an IXSS experiment leads to experimental information about diagonal elements of ε^{-1}, we should expect that transferring *two different* momenta coherently and simultaneously, the experimental outcome should be related to nondiagonal elements of ε^{-1}, that is to a quantity related to Fourier components of the potentials to different spatial periodicities. The necessary extension of the conventional scattering technique therefore is to use a superposition of two coherently coupled plane waves instead of one simple plane wave as initial photon state of the scattering process. Such a coherent superposition of two plane waves is generated when setting a perfect crystal into Bragg condition. In this case, the incoming and Bragg-reflected plane wave are coherently coupled via the nonvanishing Fourier component of the valence-electron density to a certain reciprocal lattice vector, thus forming a standing wave field. The properties of this wave field (relative amplitudes and phases) can be calculated from the dynamical theory of X-ray diffraction as a function of the exact incidence angle [5].

Figure 1 allows a comparison of the principles of IXSS experiments and the extended technique, called **C**oherent **I**nelastic **X**-Ray **S**cattering (**CIXS**). For an IXSS experiment, the incoming plane wave $\boldsymbol{k}_0$ is scattered into the direction $\boldsymbol{k}'$, transferring momentum $\boldsymbol{q} = \boldsymbol{k}_0 - \boldsymbol{k}'$ and energy $\hbar\omega = \hbar(\omega_0 - \omega')$ to the scattering system. In a CIXS experiment, the incoming wave $\boldsymbol{k}_0$ is partly Bragg-reflected, leading to a plane-wave

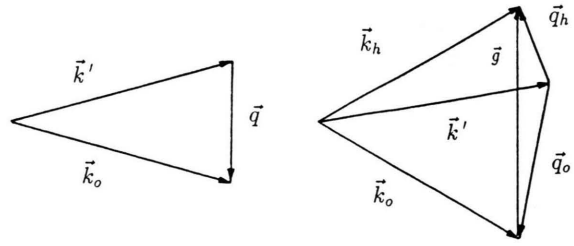

Fig. 1. Comparison of the principle of conventional and coherent inelastic scattering, IXSS and CIXS; details are given in the text.

component $\boldsymbol{k}_h$. These two plane waves are coupled via $\boldsymbol{k}_h = \boldsymbol{k}_0 + \boldsymbol{g}$, $\boldsymbol{g}$ being the reciprocal-lattice vector of the underlying Bragg-reflection. Now, two scattering contributions to $\boldsymbol{k}'$ being observed, two momenta $\boldsymbol{q}_0 = \boldsymbol{k}_0 - \boldsymbol{k}'$ and $\boldsymbol{q}_h = \boldsymbol{k}_h - \boldsymbol{k}'$ are transferred simultaneously.

Calculating the DDSCS for this type of experiment, that is, if the intensity of the primary photon field can be expressed as

$$I(\boldsymbol{r}, \Delta\phi) = A_0^2 + A_h^2 + 2|A_0|\,|A_h| \cos(\boldsymbol{g}\cdot\boldsymbol{r} + \Delta\phi), \tag{3}$$

we end up with (for a centrosymmetric crystal and introducing the simplification $|\boldsymbol{q}_0| = |\boldsymbol{q}_h|$) [6]

$$\frac{\mathrm{d}^2\sigma}{\mathrm{d}\omega\,\mathrm{d}\Omega} \sim \frac{1}{A_0^2 + A_h^2}\left(A_0^2\, S(\boldsymbol{q}_0, \omega) + A_h^2\, S(\boldsymbol{q}_h, \omega)\right)$$

$$+ \frac{2|A_0|\,|A_h|}{A_0^2 + A_h^2} \cos(\Delta\phi)\, S(\boldsymbol{q}_0, \boldsymbol{q}_h, \omega), \tag{4}$$

where A_0 and A_h are the amplitudes of the two components of the standing wave field, $\Delta\phi$ is the phase relation between both waves, and $S(\boldsymbol{q}_0, \boldsymbol{q}_h, \omega)$ is called *nondiagonal dynamic structure* factor. As we should expect, the DDSCS consists of contributions from the plane waves $\boldsymbol{k}_0$ and $\boldsymbol{k}_k$ themselves, analogous to a simple IXSS experiment (terms I and II), and of an interference term (term III) caused by the coherent coupling of $\boldsymbol{k}_0$ and $\boldsymbol{k}_k$ via $\boldsymbol{g}$. This term yields $S(\boldsymbol{q}_0, \boldsymbol{q}_h, \omega)$, a quantity obviously containing information about the coherent coupling of two quantum-mechanical excitation amplitudes. It is related to nondiagonal elements of the inverse dielectric matrix via

$$S(\boldsymbol{q}_1, \boldsymbol{q}_2, \omega) = -\frac{\hbar^2 q^2}{4\pi e^2 \varrho} \times \mathrm{Im}\, \varepsilon^{-1}_{\boldsymbol{g}_1, \boldsymbol{g}_2}(\boldsymbol{q}, \omega) \tag{5}$$

with

$$\boldsymbol{q}_1 = \boldsymbol{q} + \boldsymbol{g}_1, \quad \boldsymbol{q}_2 = \boldsymbol{q} + \boldsymbol{g}_2.$$

So we end up with an expression for the DDSCS for the CIXS experiment that contains a mixture of terms correlated to conventional inelastic scattering and an interference term containing the desired information about nondiagonal elements of ε^{-1}. The relative weight of these terms is determined by the characteristics of the initial standing wave field, i.e. by the relative amplitude and phase. The separation of the three terms can be done by using the experimental setup, shown in the next section.

3. Experimental Setup

Figure 2 shows the principles of the experimental setup used at the storage ring DORIS II at HASYLAB, Hamburg. The white synchroton radiation is monochromatized, using a Si(111)-double-crystal monochromator, to a primary energy of about 8 keV.

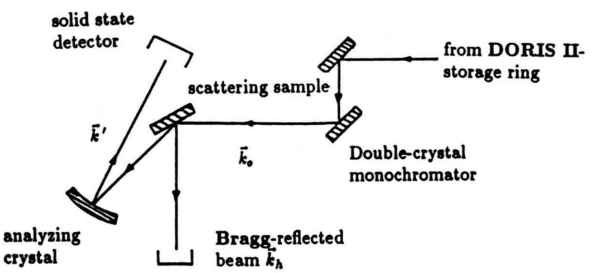

Fig. 2. The experimental setup.

The second crystal of the monochromator together with the scattering sample (also Si(111)) form a non-dispersive (+/−)-double-crystal setting. The Bragg-reflected intensity is registered by a NaI-detector, whereas the inelastically scattered radiation is energy-analysed by a spherically bent analysing crystal (Si(555)) and registered by a solid-state Ge-detector to improve the signal-to-noise ratio.

As we know from the dynamical theory of X-ray diffraction, we can calculate the amplitudes and phases of the incoming and the Bragg-reflected wave from the exact incidence angle, which in turn can be determined experimentally by measuring the Bragg-reflected intensity. So the factors that give the weights of the three contributions to the DDSCS can be manipulated by tilting the scattering sample with respect to the second monochromator crystal.

In compact notation (4) becomes

$$\frac{\mathrm{d}^2\sigma}{\mathrm{d}\omega\,\mathrm{d}\Omega} = F_1(\bar{Y})\,S(\boldsymbol{q}_0,\omega) + F_2(\bar{Y})\,S(\boldsymbol{q}_h,\omega) + F_3(\bar{Y})\,S(\boldsymbol{q}_0,\boldsymbol{q}_h,\omega), \tag{6}$$

where $\bar{Y}$ denotes a generalized incidence parameter, connected to the incidence angle. (The calculation of $F_{1,2,3}(\bar{Y})$ can be found in detail in [13].) We can see that, measuring the DDSCS for at least three different incidence angles, i.e., for three different values of $\bar{Y}$, we end up with a system of linear equations for the three contributions to the DDSCS. In this way, the nondiagonal structure factor can be extracted in principle.

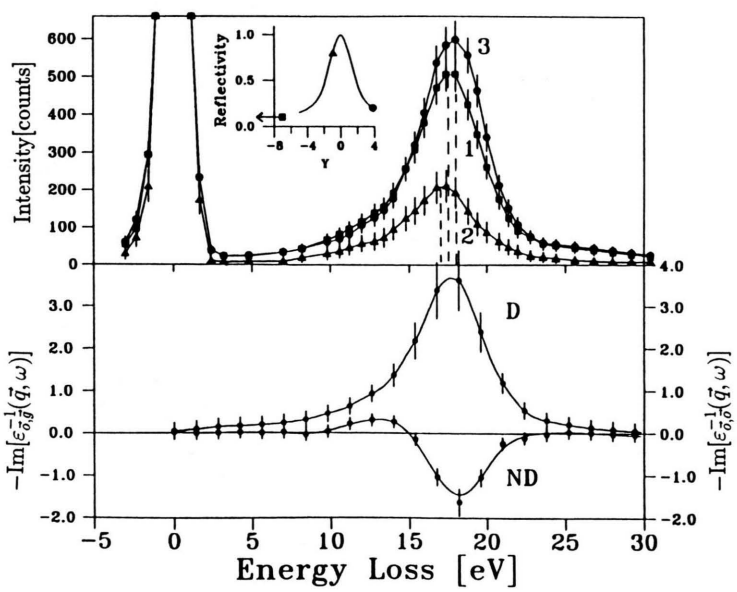

Fig. 3. Upper part: raw experimental data for Si with $|\boldsymbol{q}| = 0.51$ a.u. for three different values of $\bar{Y}$, as indicated in the inset. Vertical dashed lines indicate the centres of the spectra. Lower part: result of the separation process. D: diagonal term, ND: nondiagonal term.

In practice, in order to reduce statistical errors, we measured the DDSCS for seven different values of $\bar{Y}$ and solved the resulting overdetermined system of linear equations.

The measurements were performed for four different directions and values of $\boldsymbol{q}$ (the exact values chosen were: 0.51, 0.64, 0.76 and 1.21 a.u.). The chosen Bragg reflection was the Si(111)-reflection. In any case, the scattering geometry was chosen in a way that $|\boldsymbol{q}_0| = |\boldsymbol{q}_h|$, so that $\boldsymbol{q}_0$ always ended on different points on the $\boldsymbol{g} = \frac{2\pi}{a}(1,1,1)$ Bragg-plane.

The upper part of Fig. 3 shows the experimental raw data for $|\boldsymbol{q}_0| = 0.51$ a.u. for three different values of the incidence angle, indicated on the rocking-curve in the inset. The difference in height of these spectra is due to extinction and absorption effects, which strongly depend on the incidence angle. The influence of the interference term can be seen from the different maximum positions of the three curves. In the lower part of Fig. 3, the result of the separation process is shown. Because $\boldsymbol{q}_0$ and $\boldsymbol{q}_h$ were chosen equivalent with respect to crystal symmetry, $S(\boldsymbol{q}_0, \omega)$ and $S(\boldsymbol{q}_h, \omega)$ are identical. They show the typical plasmon line-shape, marked as curve **D**. The nondiagonal term, on the other hand, leads to a strong peak–valley structure, as can be seen from the curve labelled **ND**.

In the next section, the gained experimental results are compared with a theoretical model for the dielectric response.

4. Experimental Results vs. Theory

The experimental results shall be compared to the so-called plasmon-band model for the dielectric response of the electrons of a solid. Considering a homogeneous electron gas, we find the well-known dispersion relation for the collective excitation

$$\hbar\omega_p(q) = \hbar\omega_0 + \alpha q^2 \tag{7}$$

with ω_0 and α being the free-electron plasmon frequency and a constant depending on the electron density, respectively. As was mentioned in Section 1, turning to a spatially periodic solid means that in reciprocal space $\omega_p(\boldsymbol{q})$ is a periodic function. Backfolding into the 1st Brillouin zone yields a plasmon band structure $\omega_p^\nu(\boldsymbol{q}_r)$ with $\boldsymbol{q}_r = \boldsymbol{q} - \boldsymbol{g}_r$ [7, 4].

Following [2], the interaction of two plasmons that differ in momentum by $\hbar\boldsymbol{g}$, $\boldsymbol{g}$ being a reciprocal lattice vector, is determined by the $\boldsymbol{g}$th Fourier-component of the electron density. This can be described using the Hamiltonian

$$\hat{H}_i = \sum_{\boldsymbol{g}} \frac{4\pi e^2}{|\boldsymbol{q}|^2} \frac{4\pi e^2}{|\boldsymbol{q}+\boldsymbol{g}|^2} \frac{\boldsymbol{q}\cdot(\boldsymbol{q}+\boldsymbol{g})}{2m} \varrho(\boldsymbol{g})\, \boldsymbol{q} \cdot (\boldsymbol{q}+\boldsymbol{g})\, \hat{Q}(\boldsymbol{q})\, \hat{Q}(-\boldsymbol{q}-\boldsymbol{g}), \tag{8}$$

where $\hat{Q}(\boldsymbol{q})$ are generalized plasmon coordinates. Thus we get the following linear eigenvalue problem for the plasmon band structure $\omega_p^\nu(\boldsymbol{q}_r)$ and the eigenvector-components $A_\nu(\boldsymbol{q}_r + \boldsymbol{g}_r)$, the squared modulus of which gives the probability to find a plasmon with momentum $\hbar(\boldsymbol{q}_r + \boldsymbol{g}_r)$ and energy $\hbar\omega_p^\nu(\boldsymbol{q}_r)$:

$$[\omega_p(\boldsymbol{q}_r+\boldsymbol{g}) - \omega(\boldsymbol{q}_r)]\, A(\boldsymbol{q}_r+\boldsymbol{g}) + \sum_{\boldsymbol{g}'} C(\boldsymbol{q}_r+\boldsymbol{g}, \boldsymbol{g}')\, A(\boldsymbol{q}_r+\boldsymbol{g}') = 0 \tag{9}$$

with

$$C(\boldsymbol{q}_r+\boldsymbol{g}, \boldsymbol{g}') = \frac{4\pi e^2}{|\boldsymbol{q}_r+\boldsymbol{g}|^2} \frac{4\pi e^2}{|\boldsymbol{q}_r+\boldsymbol{g}'|^2} \cdot \frac{(\boldsymbol{q}_r+\boldsymbol{g})\cdot(\boldsymbol{q}_r+\boldsymbol{g}')}{4m} \frac{\varrho(\boldsymbol{g}'-\boldsymbol{g})}{\omega_0(\boldsymbol{q}_r+\boldsymbol{g}')}. \tag{10}$$

According to [4], i.e. assuming that only collective modes with δ-function-like energy shape are excited, the imaginary part of the related elements of the dielectric matrix can be calculated by

$$\operatorname{Im} \varepsilon^{-1}_{\boldsymbol{g}_r,\boldsymbol{g}}(\boldsymbol{q}_r, \omega) = -\frac{4\pi e^2}{|\boldsymbol{q}_r+\boldsymbol{g}_r|\,|\boldsymbol{q}_r+\boldsymbol{g}|} \cdot \sum_\nu A_\nu(\boldsymbol{q}_r+\boldsymbol{g}_r)\, A_\nu^*(\boldsymbol{q}_r+\boldsymbol{g}) \times \delta(\omega - \omega_p^\nu(\boldsymbol{q}_r)). \tag{11}$$

This equation is fundamental for the interpretation of inelastic scattering experiments in terms of the plasmon band model.

In the case of conventional IXSS, where only diagonal elements of ε^{-1} can be measured, the DDSCS turns out to be connected to $\sum_\nu |A_\nu(\boldsymbol{q})|^2$. Thus, if we try to find experimental evidence for the plasmon band structure, we have to choose the momentum transfer to lie on a Bragg plane whose corresponding reciprocal lattice vector $\boldsymbol{g}^*$ is the shortest with nonvanishing Fourier component of the electron density and is smaller than the plasmon cut-off vector. Using a simple two-plasmon-band model, we get two eigenvector components $A_{1,2}(\boldsymbol{q})$ of equal size and sign, which correspond to two plasmons the energies of which are separated by the plasmon band gap. The DDSCS then should exhibit a double-peak structure.

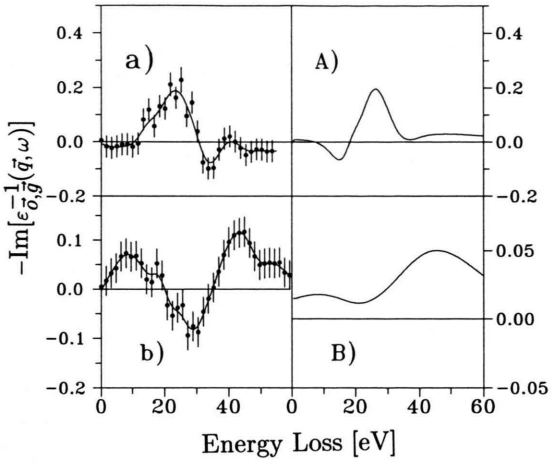

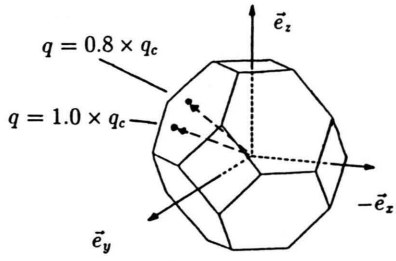

Fig. 4. *Left part:* (a, b) experimental and (A, B) corresponding model-calculated nondiagonal elements of $\varepsilon^{-1}_{\mathbf{0},\boldsymbol{g}}(\boldsymbol{q},\omega)$ with $\boldsymbol{g} = \frac{2\pi}{a}(\bar{1},\bar{1},\bar{1})$, $|\boldsymbol{q}_{(a,A)}| = 0.51$ a.u. and $|\boldsymbol{q}_{(b,B)}| = 0.64$ a.u. *Right part:* position of the $\boldsymbol{q}$-end-points on the Brillouin zone boundary.

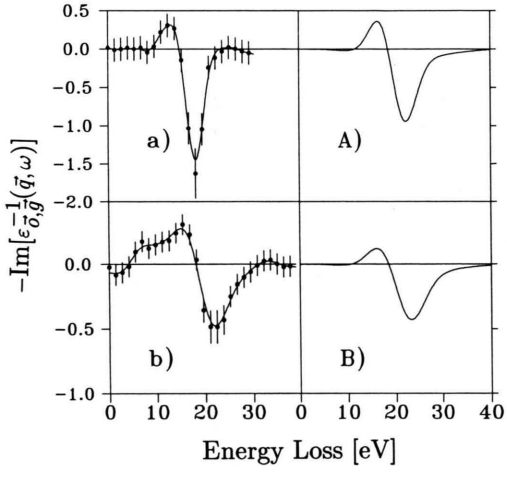

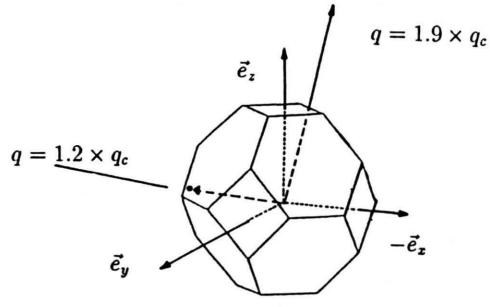

Fig. 5. *Left part:* (a, b) experimental and (A, B) corresponding model-calculated nondiagonal elements of $\varepsilon^{-1}_{\mathbf{0},\boldsymbol{g}}(\boldsymbol{q},\omega)$ with $\boldsymbol{g} = \frac{2\pi}{a}(\bar{1},\bar{1},\bar{1})$, $|\boldsymbol{q}_{(a,A)}| = 0.76$ a.u. and $|\boldsymbol{q}_{(b,B)}| = 1.21$ a.u. *Right part:* position of the $\boldsymbol{q}$-end-points on the Brillouin zone boundary.

(For the case of Si, $\boldsymbol{g}^* = \frac{2\pi}{a}(1,1,1)$, see [8].) In practice, IXSS experiments failed in detecting this double-peak structure because of the fact that the natural line-width of both plasmons is large compared to the expected energy gap.

This failure can be overcome by looking at a special nondiagonal element of ε^{-1}, namely $\varepsilon^{-1}_{\mathbf{0},\boldsymbol{g}^*}\left(\frac{\boldsymbol{g}^*}{2},\omega\right)$. Using again the two-plasmon-band model, the two products $A_1\left(\frac{\boldsymbol{g}^*}{2}\right)\cdot A_1^*\left(-\frac{\boldsymbol{g}^*}{2}\right)$ and $A_2\left(\frac{\boldsymbol{g}^*}{2}\right)\cdot A_2^*\left(-\frac{\boldsymbol{g}^*}{2}\right)$ are equal in size but different in sign, thus leading to a peak–valley structure in the DDSCS. In this type of experiment, the fingerprint of plasmon-banding should therefore be clearly seen independently of the ratio of line-width and band-gap.

Figures 4 and 5 show the obtained experimental data for four different nondiagonal elements of ε^{-1} in the left-hand part. The right-hand part shows the results of a calculation following the plasmon band model using 51 reciprocal lattice vectors. These calculations were carried out in the following way: First, the eigenvalue-problem (9) was solved, leading to the contributions of the different plasmons, which are given by the eigenvector-components. Then, for every contributing plasmon, instead of a δ-function-like energy distribution, a Gaussian-like distribution, the FWHM (Full Width at Half Maximum) of which was fitted to empirical X-Ray data [9], was added to

the DDSCS, weighted with the appropriate factor $A_v\left(\frac{\boldsymbol{g}^*}{2}\right) \cdot A_v^*\left(-\frac{\boldsymbol{g}^*}{2}\right)$. The first frequency moments of the experimental nondiagonal terms fulfil the Johnson sum-rule [10] within experimental error.

For the two measurements with $\boldsymbol{q}_0$ in the vicinity of the L-point, the conditions for the two-plasmon-band model are fulfilled (see Figure 4). The peak–valley structure, an indication for plasmon banding as stated above, can be seen clearly in the experimental and theoretical data for both measurements. It is remarkable that even for values of the momentum transfer larger than the plasmon cut-off vector, when a collective excitation should easily decay into single-particle excitations, the calculation using the plasmon band model fits the experimental results at least qualitatively.

Another way of comparison of the experimental data with theory is to calculate the elements of the dielectric matrix and perform matrix inversion. This was done in the random-phase approximation [11], [12], leading to similar results.

5. Summary

We have presented a new technique for inelastic scattering experiments that allows the measurement of nondiagonal elements of the inverse dielectric matrix. An experimental setup installed at HASYLAB was shown. The experimental results were compared to the results of a plasmon-band model for the dielectric response, finding for the first time direct experimental evidence for the existence of plasmon-banding.

This work has been funded by the German Federal Ministry of Research and Technology (BMFT) under contract No. 05 434 AXB.

[1] K. Sturm, Z. Naturforsch. **48a,** 233 (1993).
[2] P. Noziéres and D. Pines, Nuovo Cim. **9,** 470 (1958).
[3] H. S. Hybertsen and S. G. Louie, Phys. Rev. B **34,** 5390 (1986).
[4] W. M. Saslow and G. F. Reiter, Phys. Rev. B **7,** 2995 (1973).
[5] Max v. Laue, Röntgenstrahlinterferenzen, Akademische Verlagsgesellschaft, Frankfurt (Main) 1960.
[6] W. Schülke, Phys. Lett. **83 A,** 451 (1981).
[7] K. C. Pandey, P. M. Platzman, P. Eisenberger, and E-Ni Foo, Phys. Rev. B **9,** 5046 (1974).
[8] L. E. Oliveira and K. Sturm, Phys. Rev. B **22,** 6283 (1980).
[9] J. R. Schmitz, A. Kaprolat, and W. Schülke, to be published.
[10] D. L. Johnson, Phys. Rev. B **9,** 4475 (1974).
[11] R. Daling, W. van Haeringen, and B. Farid, Phys. Rev. B **44,** 2952 (1991).
[12] A. Kaprolat, Ph.D. Thesis, Universität Dortmund (1991).
[13] W. Schülke and S. Mourikis, Acta Cryst. A **42,** 86 (1986).